Modeling of Multifrequency Variability of Blazars

Andrei Sokolov* and Alan P. Marscher*

*Institute for Astrophysical Research, Boston University, 725 Commonwealth Ave., Boston, MA 02215, USA

Abstract. We model synchrotron and inverse Compton flares in blazars from radio to X-rays and gamma-rays. We take into account the internal structure and geometry of the source (energy stratification) caused by particle acceleration at shock wave fronts and synchrotron energy losses. We also consider the effects of light-travel time of the synchrotron emission that supplies the seed photons for synchrotron self-Compton scattering. These internal light-travel delays may lead to a lag of the higher energy flare with respect to variations at lower frequencies. In the model, a flare in the jet follows a collision between moving and stationary shocks. The collision leads to the creation of forward and reverse shocks, both advecting down the jet along with the shocked plasma, but moving in opposite directions in the shocked plasma rest frame. The double shock-wave structure of the emission region could be apparent in the flare profile and can provide an explanation for large time delays between synchrotron and inverse Compton flares.

SHOCK COLLISIONS

Instabilities in the inner portions of the accretion disk may lead to a deposition of large amounts of energy at the base of a relativistic jet. The speed of the deposited high energy plasma increases while its internal energy is converted into bulk kinetic energy. If the speed of the fast flow exceeds the sound speed in the quiescent plasma rest frame, the information about the incoming fast flow cannot be transmitted by sound waves in the quiescent flow. This leads to a pile-up of the quiescent plasma in front of the fast flow and the formation of a shock wave that separates the piled-up material from the quiescent flow. Similarly, the presence of a slow flow in front of the fast plasma will lead to the formation of a compression wave propagating into the fast plasma. This compression wave may steepen into a shock wave if the speed difference between fast and slow flow is large enough. A contact discontinuity separates the fast flow and the formerly quiescent material that has been piled-up in front of it. Thus, introduction of energetic plasma into the jet leads to the formation of a relativistic shell of compressed material propagating downstream.

Interaction of a relativistic jet with the ambient medium surrounding the jet may lead to the formation of stationary shock waves in the jet [1]. If the pressure in the jet is higher than that of the ambient medium, the jet will expand and then over-expand due to inertia. The pressure of the jet will eventually drop below that of the ambient medium which will launch a set of compression waves into the jet. Due to the relativistic nature of the jet one can expect the compression waves caused by pressure imbalance with the external medium to steepen into a system of oblique shock waves. Under the influence of the external medium the jet begins to contract, causing the pressure inside it to rise. Eventually it will exceed the outside pressure, once again causing the repetition of the cycle. The system of oblique shocks is expected to terminate at the center of the jet with a shock wave normal to the jet flow called a Mach disk [2]. The oscillating nature of the jet interaction with the surrounding medium may lead to multiple repetitions of the pattern of oblique shock waves and Mach disk. However, if the pressure in the surrounding medium drops with distance from the central engine, the oscillation will be damped quickly, perhaps leaving the first system of stationary shock waves the dominant feature in the quiescent jet on parsec scales.

We propose that fast term variability of blazars (on a time scale of days to weeks) can be caused by collisions between moving and stationary shock waves. The colliding shocks may be treated as shells [4]. The problem is fairly straightforward in the case of the moving shock since it is essentially a 1D structure. The Mach disk, on the other hand, is intrinsically 3D and the structure of the flow past the Mach disk must depend on the properties of the oblique shocks. The Mach disk slows down the highly relativistic upstream flow to a mildly relativistic speed ($v \leq c/\sqrt{3}$, where $c/\sqrt{3}$ is the speed of sound in a fully relativistic plasma). Most of the bulk kinetic energy of the flow going through the Mach disk is converted into internal energy of the plasma. A fraction of this energy is radiated away as synchrotron emission, giving rise to a stationary feature in the relativistic jet that can be identified with the radio core [1]. However, most of this internal energy will drive the re-acceleration of the bulk flow of the plasma. The shell associated with the Mach

disk is confined between the shock itself and the approximate position of the onset of expansion downstream of the Mach disk.

The collision of two shells leads to the formation of a characteristic doubly structured emission region consisting of two zones separated by a contact discontinuity and confined between two transmitted shocks (forward and reverse shocks). Emission from each zone will produce a flare that starts at the moment of collision and ceases when the relevant shock reaches the boundary of the emission zone, whose position depends on the thickness of the shells. The bulk plasma speed and pressure are continuous across the contact discontinuity. The speed of the shocked plasma is determined by the speed of the moving shock and the quiescent flow (the Mach disk is assumed to be stationary). We derived an approximate formula for the Lorentz factor of the shocked plasma:

$$\Gamma_p = 0.5\Gamma_s/\Gamma_q, \tag{1}$$

where Γ_s is the Lorentz factor of the moving shock front and Γ_q is that of the quiescent flow upstream of the Mach disk. One can see that in order to achieve $\Gamma_p = 10$ for the shocked material, $\Gamma_s = 200$ is required if $\Gamma_q = 10$. Such high speeds are not unusual in gamma-ray bursts [3] and could occur in active galactic nuclei. Shocked plasma at $\Gamma_p \sim 10$ may be identified with the superluminal features one can see emanating from the radio core in multi-epoch VLBI images. A collision with an energetic shock wave is likely to destroy the Mach disk, but the stationary structure is expected to re-establish itself quickly after the passage of a moving shock.

INTERNAL STRUCTURE AND LIGHT TRAVEL EFFECTS

Synchrotron emission from both forward and reverse zones can be calculated separately for optically thin frequencies of observation. The observed flux during the flare is obtained from solving time-dependent radiative transfer equations through the highly inhomogeneous evolving medium consisting of relativistic particles accelerated by a shock wave. Electrons accelerated to the highest energies by the shock wave radiate away their energy and begin to decay as soon as they leave the acceleration region at the shock wave front. This introduces a strong gradient in the distribution function of the accelerated particles across the excitation region. Furthermore, emission produced at the near side of the source will reach the observer earlier than the emission produced at the far side of the source. These light travel delays must be taken into account in solving the radiative transfer problem in order to calculate the observed flux correctly.

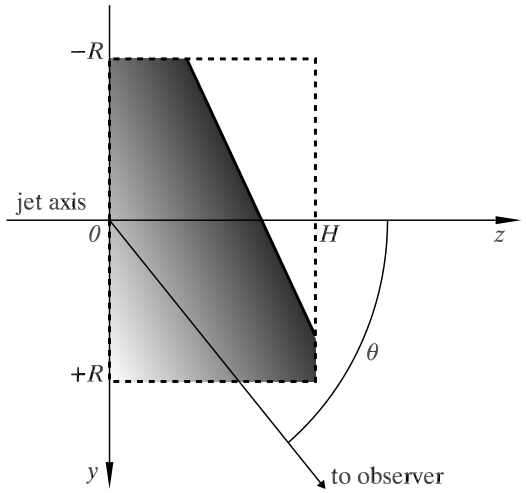

FIGURE 1. External apparent shock wave structure for viewing angle θ in the plasma rest frame. The axis of the jet corresponds to the z-axis. The external observer is assumed to be in the y-z plane. The forward region shown is assumed to be a cylinder oriented along the jet axis. A cross-section of the excitation region is shown.

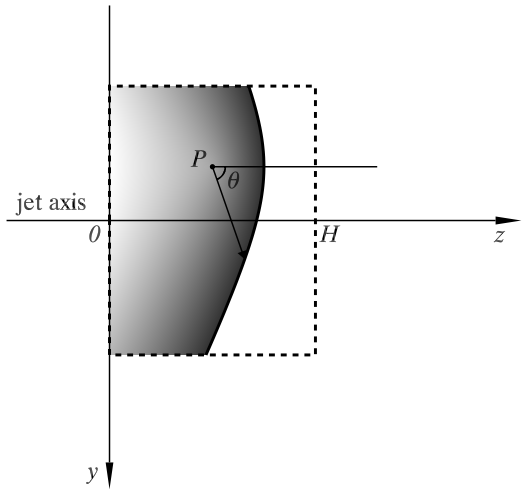

FIGURE 2. Internal apparent shock wave structure as viewed from an arbitrary point P inside the source. A cross-section of the excitation region parallel to the y-z axis is shown. The distance between point P and the internal apparent shock position at an arbitrary angle θ to the z-axis depends upon the travel time from this position to point P.

The forward region is shown in Fig. 1 with a dashed outline. The solid line indicates the orientation of the apparent shock wave front as seen by an observer at viewing angle θ in the plasma rest frame. The near side of the source (bottom in Fig. 1) is shown to be fully excited, whereas significant portions of the far side of the source (top) have not yet been reached by the apparent shock front because of light travel delays across the excitation region. The gray-scale gradient across the region of the source covered by the apparent shock corresponds to the gradient in the maximum energy of the accelerated electrons producing synchrotron emission, $E_{max} = \gamma_{max} m_e c^2$, where m_e is the mass of electron. Higher energy synchrotron emission arrives from darker regions; lighter areas correspond to lower energy emission.

Calculating inverse Compton emission presents the greatest difficulty when light travel effects are fully included in the modeling. Besides external light travel effects similar to those considered in the synchrotron emission calculation, one has to consider the internal light travel effects as well. In the synchrotron self-Compton model, synchrotron emission produced in the source provides the seed photons for the inverse Compton scattering. Synchrotron emission at a given location in the excitation region at a particular time arrives from the volume of the source bounded by the internal apparent shock front, an example of which is shown in Fig. 2. The travel time across the excitation region is comparable to the shock wave crossing time and, therefore, the synchrotron seed photons may arrive at a given location with a significant time delay that may translate into a time delay of the observed inverse Compton flare compared to its synchrotron counterpart. The effect is even more significant if synchrotron emission from the adjacent region is included (adjacent region is not shown in Fig. 2).

MODEL PROPERTIES

We have developed a code that simulates the observed emission for a set of input parameters that describe the emission region geometry, shock wave speed, distribution of accelerated electrons, and the observer distance and viewing angle. For the sake of simplicity we consider the properties of the light curves in the rest frame of the emitting plasma in this section. The observed light curves can be calculated easily from the plasma rest frame results provided that the speed of the shocked plasma Γ_p and the redshift of the active galaxy hosting the jet are specified. The light curves depend strongly on the angle of observation. In this paper we only consider a viewing angle $\theta = 90^\circ$ in the plasma rest frame. This viewing angle maximizes the apparent speed of the superluminal components for a constant bulk Lorentz factor of the jet

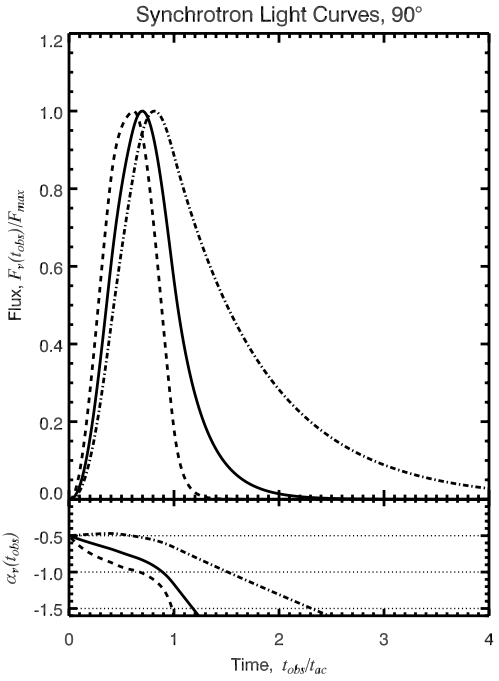

FIGURE 3. Synchrotron light curves for viewing angle $\theta = 90^\circ$ in the plasma rest frame. The rest-frame frequencies of observation used are 2×10^{10} Hz (dot-dashed), 2×10^{11} Hz (solid), and 2×10^{12} Hz (dashed). The evolution of the spectral index α, defined as $F_\nu \propto \nu^\alpha$, is shown in the bottom panel.

Γ_p. Due to the highly relativistic speed of the emitting plasma, the viewing angle of 90° corresponds to a very small angle of observation $\theta' \approx 1/\Gamma_p$ in the observer frame, which for $\Gamma_p = 10$ is $\theta' \approx 6^\circ$.

We present the results of the synchrotron emission calculations in Fig. 3, showing normalized flux at three representative frequencies as a function of the observer time t_{obs} normalized by the apparent crossing time t_{ac}. For $\theta = 90^\circ$ the apparent crossing time is

$$t_{ac} = 2R/c + H/(c\beta), \tag{2}$$

where β is the speed of the shock in the plasma rest frame. The shapes of the observed light curves can be understood by comparing the apparent crossing time t_{ac} and the synchrotron emission decay time,

$$t_\nu^{syn} = \frac{7.8 \times 10^8 \,\mathrm{sec}}{(B/1\,\mathrm{G})^2 \gamma_{max}} \left(\frac{\nu_{max}}{\nu}\right)^{1/2}, \tag{3}$$

where B is magnetic field strength, γ_{max} is the maximum Lorentz factor of electron distribution, and $\nu_{max} = c_1 B \gamma_{max}^2$ ($c_1 = 2.8 \times 10^6$ in cgs units). If the decay time is

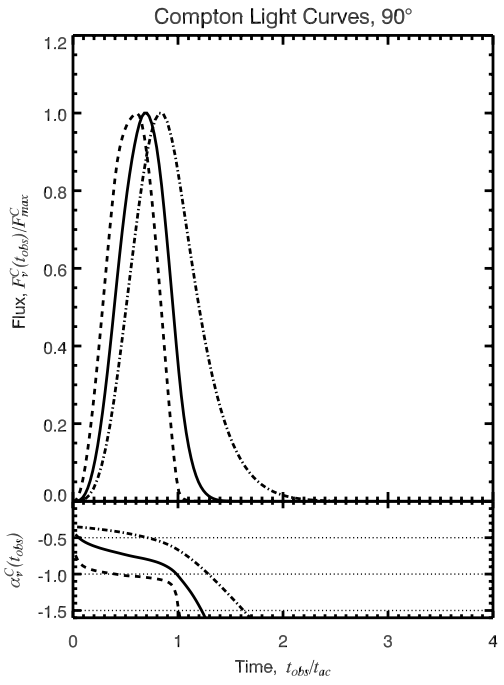

FIGURE 4. Inverse Compton light curves for viewing angle $\theta = 90^\circ$ in the plasma rest frame. The frequencies used are 2×10^{14} Hz (dot-dashed), 2×10^{16} Hz (solid), and 2×10^{20} Hz (dashed).

much greater than the apparent crossing time, then the synchrotron flare appears highly asymmetric with relatively fast rise time and long exponential decay. The flares are symmetric if the reverse is true. Indeed, for a short decay time the emission region is confined to a finite volume behind the apparent shock wave front. In this case the observed flare will trace the geometry of the source as it is being traversed by the apparent shock front. The geometry is roughly circular for viewing angle $\theta = 90^\circ$ (see Fig. 1). Flares at relatively high frequencies, i.e., larger than the critical frequency defined by $t_\nu = t_{ac}$, are expected to peak at $\sim 1/2 t_{ac}$ as this is the time when the extent of the excited region is the largest at these frequencies. At low frequencies the flares are expected to grow until $t_{obs} \approx t_{ac}$ because the excited region fills up the whole source behind the apparent shock front. The emission at low frequencies grows with the increasing volume of the excited region.

Inverse Compton flares are presented in Fig. 4 along with the spectral index evolution during the flare. The decay time of the inverse Compton emission cannot be defined as easily as in the case of the synchrotron emission because it not only depends on the electron energy distribution but also on the incident spectrum of the internal synchrotron emission whose properties depend strongly on position in the source, direction, and time. Nonetheless, assuming that the incident emission extends up to the highest possible frequencies for the maximum γ_{max}, one can use the following expression for the inverse Compton decay time:

$$t_\nu^{com} = \frac{7.8 \times 10^8 \,\mathrm{sec}}{(B/1\,\mathrm{G})^2 \gamma_{max}} \left(\frac{4\gamma_{max}^2 \nu_{max}}{\nu} \right)^{1/2}. \qquad (4)$$

The basic behavior of the inverse Compton light curves is similar to that of synchrotron emission. However, inverse Compton flares tend to be symmetric even at relatively low frequencies because the flares are quenched quickly due to fast decline in ν_{max} when the internal apparent shock leaves the excitation region and the maximum energy electrons are no longer produced. Depending on the frequency of observation, both negative and positive time delays between synchrotron and inverse Compton flares can be observed.

Emission from both forward and reverse regions will be a combination of two flares. For the viewing angle $\theta = 90^\circ$, the flares are indistinguishable if the emission regions are described by identical sets of input parameters. Any difference in electron density n or minimum Lorentz factor of electrons γ_{min} will not affect the shapes of the flares but the peak levels of emission will be different. However, changing the extent of one of the emission regions along the jet axis will result in different crossing times for this region. In this case, one event, i.e., a shock wave collision, will lead to a profile of both synchrotron and inverse Compton emission consisting of two peaks with different time scales. In particular, the model predicts that a profile consisting of a relatively sharp spike of emission followed by a prolonged outburst may occur.

ACKNOWLEDGMENTS

This research was supported through NASA grant NAG5-11811 and National Science Foundation grant AST-0098579.

REFERENCES

1. Daly, R. A., and Marscher, A. P., *Astrophys. Journal*, **334**, 539-551 (1988)
2. Courant, R., and Friedrichs, K. O., *Supersonic Flow and Shock Waves*, Interscience Publishers Inc., New-York, 1948
3. Mészáros, P., *Annu. Rev. Astron. Astrophys.*, **40**, 137-169 (2002)
4. Spada, M., Ghisellini, G., Lazzati, D., and Celotti, A., *Mon. Not. R. Astron. Soc.*, **325**, 1559-1570 (2001)